Acta Cryst B
STRUCTURAL SCIENCE
CRYSTAL ENGINEERING
MATERIALS
ISSN 2052-5206

Investigation of thermal behavior of mixed-valent iron borates vonsenite and hulsite containing $[OM_4]^{n+}$ and $[OM_5]^{n+}$ oxocentred polyhedra by *in situ* high-temperature Mössbauer spectroscopy, X-ray diffraction and thermal analysis

Received 12 March 2020
Accepted 15 May 2020

Edited by R. Černý, University of Geneva, Switzerland

Keywords: oxoborate; oxidation; high-temperature Mössbauer spectroscopy; high-temperature X-ray diffraction; thermal expansion.

Supporting information: this article has supporting information at journals.iucr.org/b

Yaroslav P. Biryukov,[a] Almaz L. Zinnatullin,[b] Rimma S. Bubnova,[a] Farit G. Vagizov,[b] Andrey P. Shablinskii,[a] Stanislav K. Filatov,[c]* Vladimir V. Shilovskikh[d] and Igor V. Pekov[e]

[a]Institute of Silicate Chemistry of the Russian Academy of Sciences, Makarova emb., 2, Saint Petersburg, 199034, Russian Federation, [b]Kazan Federal University, Kremlyovskaya Str., 18, Kazan, 420008, Russian Federation, [c]Institute of Earth Sciences, Department of Crystallography, Saint Petersburg State University, Universitetskaya Emb., 7/9, Saint Petersburg, 199034, Russian Federation, [d]Geomodel Resource Centre, Saint Petersburg State University, Ulyanovskaya Str., 1, Saint Petersburg, 198510, Russian Federation, and [e]Faculty of Geology, Moscow State University, Leninskie Gory, 1, Moscow, 119991, Russian Federation. *Correspondence e-mail: s.filatov@spbu.ru

The investigation of elemental composition, crystal structure and thermal behavior of vonsenite and hulsite from the Titovskoe boron deposit in Russia is reported. The structures of the borates are described in terms of cation-centered and oxocentred polyhedra. There are different sequences of double chains and layers consisting of oxocentred $[OM_4]^{n+}$ tetrahedra and $[OM_5]^{n+}$ tetragonal pyramids forming a framework. Elemental composition was determined by energy-dispersive X-ray spectroscopy (EDX). Oxidation states and coordination sites of iron and tin in the oxoborates are determined using Mössbauer spectroscopy and compared with EDX and X-ray diffraction data (XRD). According to results obtained from high-temperature Mössbauer spectroscopy, the Fe^{2+} to Fe^{3+} oxidation in vonsenite and hulsite occurs at approximately 500 and 600 K, respectively. According to the **high-temperature** XRD data, this process is accompanied by an assumed deformation of crystal structures and subsequent solid-phase decomposition to hematite and warwickite. It is seen as a monotonic decrease of volume thermal expansion coefficients with an increase in temperature. A partial magnetic ordering in hulsite is observed for the first time with $T_c \simeq 383$ K. Near this temperature, an unusual change of thermal expansion coefficients is revealed. Vonsenite starts to melt at 1571 K and hulsite **starts to melt[melts]** at 1504 K. Eigenvalues of thermal expansion tensor are calculated for the oxoborates as well as **a character of anisotropy of the expansion[?]** is described in comparison with their crystal structures.

1. Introduction

Vonsenite and hulsite are minerals with an **approved[?]** end-member formula $Fe^{2+}{}_2Fe^{3+}(BO_3)O_2$, which were discovered over a hundred years ago (Knopf & Schaller, 1908; Eakle, 1920). Generally, these mixed-valent iron oxoborates occur in **magnesian[magnesium?]** skarns (Aleksandrov, 1998). However, the end-member formula does not adequately reflect the empirical elemental composition of these compounds that typically contain in **both Fe^{2+}- and Fe^{3+}-dominant sites admixed cations**[?] in significant amounts (Konnert *et al.*, 1976). Idealized formulae of hulsite and vonsenite are $(Mg,Fe^{2+})_2(Fe^{3+},Sn)(BO_3)O_2$ and $Fe^{2+}{}_2Fe^{3+}(BO_3)O_2$, respectively (Konnert *et al.*, 1976; Yamnova *et al.*, 1978; Swinnea & Stein-

fink, 1983). Vonsenite crystallizes in ludwigite structure type in the orthorhombic space group *Pbam* and hulsite crystallizes in pinakiolite structure type in the monoclinic space group *P*2/*m*. Although the structures are different, both minerals belong to a family of 3 Å wallpaper structure compounds (Moore & Araki, 1974; Hawthorne, 2014). The crystal structure of vonsenite contains four positions for cations: *M*(1) (2*a*) and *M*(3) (4*g*) positions are occupied by Fe^{2+} and Mg, *M*(2) (2*d*) positions are occupied by $Fe^{2.5+}$, *M*(4) (4*h*) positions are occupied by Fe^{3+} and Sn^{4+} (Swinnea & Steinfink, 1983). There are five octahedral positions for cations in the structure of hulsite: *M*(1) (1*a*) and *M*(3) (1*d*) are filled by Mg, Fe^{3+} and Sn^{4+}, *M*(2) (1*f*) and *M*(5) (2*n*) are filled by Fe^{2+} and Mg, *M*(4) (1*g*) are filled by Fe^{2+} (Yamnova *et al.*, 1978). The structures are composed of metal–oxygen octahedra and $[BO_3]^{3-}$ triangles (Takéuchi, 1956; Konnert *et al.*, 1976; Yamnova *et al.*, 1978; Swinnea & Steinfink, 1983).

Magnetic properties of iron borates strongly depend on their structure. Magnetic iron atoms form three ladder-like structures in ludwigite-like compounds. Therefore, magnetic properties of these compounds show strong unidirectional anisotropy (Whangbo *et al.*, 2002; Vallejo & Avignon, 2007; Freitas *et al.*, 2009). On the other hand, metal atoms form quasiplanar structures in pinakiolite-like compounds. Such structures determine the two-dimensional character of magnetic properties, which is different from the one described for ludwigite-like structures (Freitas *et al.*, 2010; Medrano *et al.*, 2018). Recently, it has been shown that compounds that crystallize in the ludwigite type are antiferromagnets whose structures contain magnetic arrangements with geometric frustrations (Knyazev *et al.*, 2019). 'Geometrically frustrated antiferromagnets' is one of the most intensively studied topics in condensed matter physics due to the attractive magnetic properties they exhibit (Greedan, 2001, 2010; Gomonay & Loktev, 2014; Bovo *et al.*, 2018).

There are few works known to date devoted to the investigation of the Mössbauer effect in vonsenite and hulsite. The ^{57}Fe Mössbauer spectrum recorded at room temperature of a synthetic analog of vonsenite is seen to contain several paramagnetic components (doublets) assigned to various crystallographic sites (Swinnea & Steinfink, 1983). With a decrease in temperature, a charge ordering **and a few** magnetic transitions were detected, and the spectra became more complex (Douvalis *et al.*, 2002; Larrea *et al.*, 2004). There are few articles which report high-temperature Mössbauer experiments of vonsenite (Li *et al.*, 1994; Douvalis *et al.*, 2002; Larrea *et al.*, 2004). However, an investigation of the ^{119}Sn Mössbauer effect in vonsenite has not yet been reported. In contrast, results of investigations of the ^{119}Sn Mössbauer effect in hulsite have been reported (Smith & Zuckerman, 1967; Konnert *et al.*, 1976). The ^{119}Sn Mössbauer spectrum of hulsite shows a single absorption line with isomer shift characteristic of the Sn^{4+} state. To date, there are no works known devoted to the investigation of the ^{57}Fe Mössbauer effect in hulsite.

It should be noted that there is a lack of high-temperature crystal-chemical investigations of iron borates in general. There are **a few works** known devoted to such investigations (Shimomura *et al.*, 2007; Biryukov *et al.*, 2016, 2018). A combination of *in situ* high-temperature Mössbauer spectroscopy and **high-temperature** X-ray diffraction (HTXRD) works well to reveal magnetic phase transitions in iron borates (Biryukov *et al.*, 2016, 2018). The investigation of Fe^{2+} to Fe^{3+} oxidation, which should occur in vonsenite and hulsite with an increase in temperature using data of these methods, is of special interest too.

This paper reports on the investigation of chemical composition, cation distribution and crystal structure, thermal behavior of the mixed-valent iron oxoborates vonsenite and hulsite from the Titovskoe boron deposit (Russia) by *in situ* high-temperature Mössbauer spectroscopy, HTXRD and thermal analysis [differential scanning calorimetry (DSC) and thermogravimetry (TG)]. A discussion on thermal expansion of the borates under consideration is given in terms of cation- and oxocentred polyhedra since they compose the $[OM_4]^{n+}$ tetrahedra (Krivovichev *et al.*, 1998, 2013) and $[OM_5]^{n+}$ tetragonal pyramids that are not described elsewhere for these minerals.

2. Experimental

2.1. Materials

The minerals were collected from the Titovskoe boron deposit, Tas-Khayakhtakh Range, Polar part of Sakha (Yakutia) Republic, Russia. Crystals of vonsenite suitable for single-crystal X-ray diffraction experiments were **separated from the probes[?]** using a **LOMO (Russia) binocular microscope** and then checked on a Bruker SMART APEX II diffractometer. Polycrystalline samples of the minerals were used for the room- and high-temperature Mössbauer spectroscopy, X-ray diffraction and thermal analysis experiments.

2.2. Energy-dispersive X-ray spectroscopy (EDX)

The samples were mounted in an epoxy block and polished with progressively **smaller[finer]** diamond powders up to 0.25 µm. Elemental compositions of the samples were determined using a scanning electron microscope Hitachi S3400N equipped with an energy-dispersive spectrometer Oxford X-Max 20. Operating conditions were set at 20 kV, 1 nA and 120 seconds per point dwell time. Concentrations of elements with an atomic number higher than carbon were determined. Spectra were processed **with *AZtec* (Oxford Instruments, 2016)** software using a TrueQ technique. The standards used were FeS_2 (Fe), MgO (Mg), Mn (Mn), Al_2O_3 (Al), Ti (Ti) and Sn (Sn).

Mean analytical results are given in Table S1. These data are in agreement with elemental compositions of vonsenite and hulsite from the Titovskoe deposit obtained by Aleksandrov (1998). Empirical formulae of vonsenite and hulsite based on five oxygen atoms per formula unit (apfu) are $(Fe^{2+}_{1.86}Mg_{0.13})_{\sum 1.99}(Fe^{3+}_{0.92}Mn^{2+}_{0.05}Sn^{4+}_{0.02}Al_{0.02})_{\sum 1.01}(BO_3)O_2$ and $(Fe^{2+}_{1.90}Mg_{0.11})_{\sum 2.01}(Fe^{3+}_{0.88}Mn^{2+}_{0.06}Sn^{4+}_{0.05}Al_{0.01})_{\sum 1.00}(BO_3)O_2$, respectively. Manganese **is considered to be** Mn^{2+}**, tin is considered to be** Sn^{4+} and Fe^{2+}/Fe^{3+} ratios are

Table 1
Experimental details for vonsenite at 293 and 400 K- TAKEN FROM CIF. DIFFERENCES HIGHLIGHTED.

	293 K	400 K
Crystal data		
Chemical formula	$BFe_{2.654}Mg_{0.346}O_5$	$BFe_{2.654}Mg_{0.346}O_5$
M_r	247.4	247.4
Crystal system, space group	Orthorhombic, *Pbam*	Orthorhombic, *Pbam*
a, *b*, *c* (Å)	9.3914 (10), 12.3034 (10), 3.0697 (6)	9.425 (1), 12.3528 (10), 3.0799 (6)
V (Å^3)	354.69 (8)	358.58 (8)
Z	4	4
Radiation type	Mo *Kα*	Mo *Kα*
μ (mm^{-1})	**10.70**	**10.59**
Crystal size (mm)	**0.4** × 0.1 × 0.1	**0.4** × 0.1 × 0.1
Data collection		
Diffractometer	Bruker Smart APEX II	Bruker Smart APEX II
Absorption correction	Multi-scan (Krause *et al.*, 2015)	Multi-scan (Krause *et al.*, 2015)
T_{min}, T_{max}	0.820, 0.870	0.820, 0.870
No. of measured, independent and observed [$I > 3\sigma(I)$] reflections	1886, 404, 329	1882, 404, 337
R_{int}	0.037	0.086
(sin $\theta/\lambda)_{max}$ (Å^{-1})	0.616	0.614
Refinement		
$R[F^2 > 2\sigma(F^2)]$, $wR(F^2)$, *S*	0.036, 0.039, 1.66	0.029, 0.032, 1.48
No. of reflections	404	404
No. of parameters	**57**	57
No. of restraints	1	1
$\Delta\rho_{max}$, $\Delta\rho_{min}$ (e Å^{-3})	1.02, −0.81	0.54, −0.58

calculated and these data are in accordance with the Mössbauer spectroscopy data.

2.3. Mössbauer spectroscopy

Mössbauer experiments were performed in transmission geometry using a conventional spectrometer (WissEl, Germany) operating in constant acceleration mode equipped with a Mössbauer Furnace MBF-1100 and temperature controller TR55. Low-temperature measurements were carried out with a continuous flow cryostat (model CFICEV from ICE Oxford, UK). Measurements were provided within the temperature range of 100–745 K. The ^{57}Co (Rh) with an activity of about 50 mCi and the ^{119m}Sn ($CaSnO_3$) with an activity of about 15 mCi (both RITVERC GmbH, Russia) were used as **a source[sources?] for** resonance radiation. The spectrometer velocity scale was calibrated using thin metallic iron foil (at room temperature). *SpectrRelax* software (Matsnev & Rusakov, 2012) was used for experimental data processing. Isomer shifts were measured relative to α-Fe at room temperature for ^{57}Fe Mössbauer spectra and SnO_2 at room temperature for ^{119}Sn Mössbauer spectra.

2.4. Thermal analysis

Thermal analysis (TG+DSC) was carried out using a STA 429 D NETZSCH simultaneous thermal analysis instrument equipped with a platinum–rhodium sample holder (dynamic air atmosphere, air flow 50 cm^3 min^{-1}, temperature range 313–1650 K, heating rate 20 K min^{-1}). Before the experiment, calibration of a thermobalance was made using a $CaC_{24}{\cdot}2H_2O$ external standard. The accuracy of the determination of the weight was ±0.01 mg. The temperature (K) and sensitivity (μV mW^{-1}) calibration of the Type S thermocouple was performed using In, Sn, Bi, Zn, Al, Au and Pb external standards. The errors in determinations of the temperature and sensitivity did not exceed ±2 K and ±2 relative percent, respectively. The pellets for the experiments were weighed with an accuracy of 0.01 mg (the mass was approximately 20 mg) and placed in an open platinum–rhodium crucible. The temperatures of thermal effects were determined using NETZSCH *Proteus* software **by the DSC first derivative curve[?]**.

2.5. Room- and high-temperature X-ray diffraction

Powder diffraction data were collected using a Rigaku MiniFlex II diffractometer (Co *Kα*, 2θ = 5–70°, step 0.02°). The phase composition was determined using *PDXL* integrated X-ray powder diffraction software (Sasaki *et al.*, 2010) and *PDF-2 2016* from the ICDD [ICSD] (Inorganic Crystal Structure Database, http://www2.fiz-karlsruhe.de/icsd_home.html; **Reference?**). The Rietveld refinement of the XRD patterns was performed using *RietToTensor* (Bubnova *et al.*, 2018). X-ray phase analysis revealed that the polycrystalline samples of vonsenite and hulsite contained in its compositions diopside $CaMg(Si_2O_6)$ (about 2 and 10 wt%, respectively) and Fe_3O_4 (about 0.6 wt%) as an impurities according to the Rietveld refinement.

Single-crystal X-ray diffraction data were collected using a Bruker SMART APEX II diffractometer equipped with a CCD detector using Mo *Kα* radiation and an Oxford Cobra Cryosystem device. The room- and high-temperature experi-

ments were performed using the same crystal. More than one hemisphere of three-dimensional data was collected by the CCD detector and frame widths **of 0.5°** in ω, with 30 s used to acquire each frame. The data were corrected for Lorentz, polarization and background effects using *APEX* (Bruker, 2012) and *XPREP* (Bruker, 2012). A semi-empirical absorption-correction based on the intensities of equivalent reflections was applied in the *SADABS* program (Krause *et al.*, 2015). The crystal structure of vonsenite was solved by charge flipping and refined at 293 and 400 K using *JANA2006* (Petříček *et al.*, 2014) program suite. Experimental details are given in Table 1. Atomic coordinates, displacement parameters and selected bond distances are given in Tables S2–S4. Hulsite forms very thin and curved plates, dimensions of this curvature are smaller than optical resolution of the binocular, thus it was not possible to refine the structure using a single-crystal X-ray diffraction experiment. Here the cation distribution in hulsite was determined using room-temperature Mössbauer spectroscopy data and the model of hulsite presented by Yamnova *et al.* (1978) (Tables S5–S7).

The HTXRD experiments were conducted using a Rigaku Ultima IV diffractometer with a thermal attachment (Co $K\alpha$, 40 kV and 35 mA, reflection geometry, D/teX Ultra high-speed detector, air atmosphere, 2θ = 10–80°, temperature range 293–1273 K, steps 10 and 20 K, heating rate 1.5 K min^{-1}). A thermocouple was used to control the temperature. Before the HTXRD experiment, an Si external standard was measured in the temperature range 293–1273 K in order to control the thermal expansion coefficients. The temperatures of phase transitions were checked using SiO_2 and K_2SO_4. The error in the determination of the temperature did not exceed ±10 K. Experimental data processing by the Rietveld refinement, approximation of temperature dependencies of lattice parameters and drawing figures of thermal expansion coefficients (α) were performed using *RietTo-Tensor* (Bubnova *et al.*, 2018). A detailed description of the data processing and calculation of eigenvalues of thermal expansion tensor is given in detail by Bubnova *et al.* (2018).

The crystal structures were visualized using *VESTA* (Momma & Izumi, 2011).

3. Results

3.1. Mössbauer spectroscopy

3.1.1. Room-temperature ^{119}Sn Mössbauer spectroscopy. The room-temperature ^{119}Sn Mössbauer spectrum of vonsenite [Fig. 1(*a*)] is a doublet with an isomer shift value equal to 0.17 mm s^{-1}, quadrupole splitting and linewidth equal to 0.93 and 0.8 mm s^{-1}, respectively. The values of hyperfine parameters show that the oxidation state of tin atoms is 4+. The hyperfine parameters of tin nuclei in vonsenite are reported here for the first time, which are close to those of ludwigite-like $Co_5Sn(O_2BO_3)_2$ (Medrano *et al.*, 2015).

The room-temperature ^{119}Sn Mössbauer spectrum of hulsite [Fig. 1(*b*)] is consisted of one quadrupole doublet with an isomer shift value equal to 0.23 mm s^{-1}, quadrupole splitting and linewidth equal to 0.95 and 1.07 mm s^{-1}, respectively. These values indicate Sn^{4+} atoms. The values are different from those reported for hulsites (Smith & Zuckerman, 1967; Aleksandrov *et al.*, 1967), where a single absorption line was described. However, these values of hyperfine parameters are close to those of $Ni_{5.15}Sn_{0.85}(O_2BO_3)_2$ crystallizing in pinakiolite structure type, and it was concluded that the Sn^{4+} atoms substitute several cationic positions (Medrano *et al.*, 2018). A similar conclusion was also made by Suknev & Diman (1975) based on IR studies of hulsite. The larger value of the linewidth of the spectrum of hulsite in comparison to that of vonsenite may be due to a substitution of the largest number of non-equivalent crystallographic positions by the tin atoms in the crystal structure of hulsite.

3.1.2. Vonsenite. The ^{57}Fe Mössbauer spectra of vonsenite at selected temperatures are shown in Fig. 2. These spectra were fitted with four paramagnetic components (doublets). These components correspond to four non-equivalent crystallographic positions of iron atoms in the structure of vonsenite: 2*a* [*M*(1)], 2*d* [*M*(2)], 4*g* [*M*(3)] and 4*h* [*M*(4)]. The spectrum at room temperature and its components are shown in Fig. 2(*b*).

The behavior of hyperfine parameters with temperature is shown in Fig. 3. Generally, isomer shift decreases with an increase in temperature [Fig. 3(*a*)]. However, for two components with higher values of isomer shift, *i.e.* for the Fe^{2+} atoms, an abrupt change of values of the isomer shift is seen at the temperature of about 500 K, which is due to the oxidation of Fe^{2+} atoms. At higher temperatures, values of the isomer shift of these components are characteristic of those of the

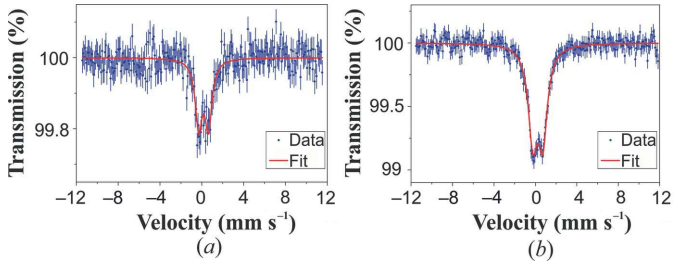

Figure 1
^{119}Sn Mössbauer spectra of (*a*) vonsenite and (*b*) hulsite recorded at room temperature.

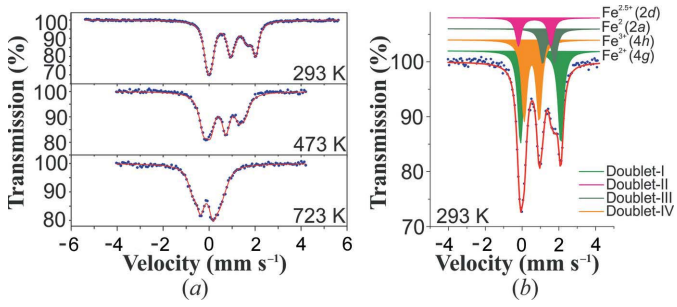

Figure 2
^{57}Fe Mössbauer spectra of vonsenite (*a*) at 293, 473 and 723 K and (*b*) its spectral components at 293 K.

Fe^{3+} atoms. Values of quadrupole splitting indicate the octahedral coordination of the cations throughout the whole temperature range [Fig. 3(*b*)].

3.1.3. Room- and high-temperature ^{57}Fe Mössbauer spectroscopy of hulsite. The room-temperature ^{57}Fe Mössbauer spectrum of hulsite can be fitted with one magnetically split (sextet) and two paramagnetic (doublets) components (Fig. 4).

Values of hyperfine parameters of the magnetically split component [orange curve (I) in Fig. 4] are characteristic of the Fe^{3+} atoms occupying highly distorted octahedral sites. It is assumed that these are the 1*d* and 1*g* positions. As the temperature increases, a hyperfine field on iron nuclei decreases with a subsequent transformation of the magnetically split component into the paramagnetic doublet near the

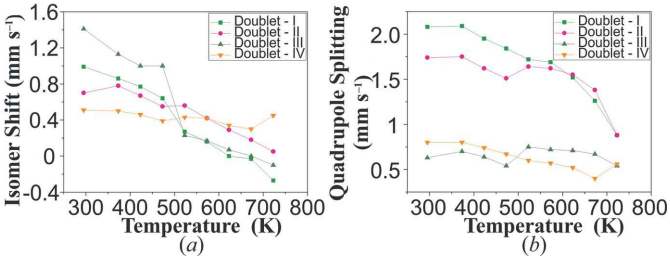

Figure 3
Temperature dependencies of the hyperfine parameters of the ^{57}Fe Mössbauer spectral components of vonsenite: (*a*) isomer shift and (*b*) quadrupole splitting.

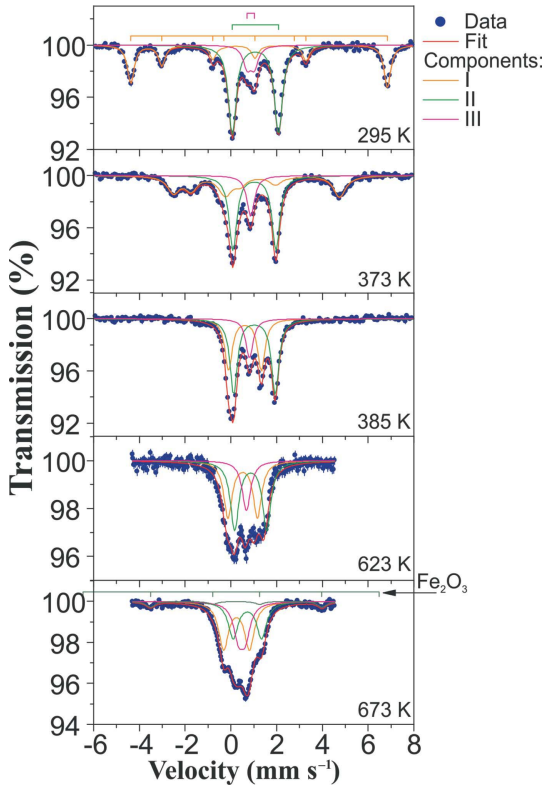

Figure 4
^{57}Fe Mössbauer spectra of hulsite at 295, 373, 385, 623 and 673 K.

critical temperature, T_c [Fig. 5(*a*)]. Such a partial magnetic ordering **should be caused[?]** by the quasi-two-dimensional structure of hulsite. Below the critical temperature, some of these planes are magnetically ordered, while others are not ordered. Similar behavior was observed in other pinakiolite-like compounds (Freitas *et al.*, 2010; Medrano *et al.*, 2018). The experimental data on the temperature dependence of the ^{57}Fe hyperfine field in hulsite were least-squares fitted by power law:

$$B_{HF}(T) = B_{HF}(0)\left(1 - \frac{T}{T_c}\right)^{\beta} \quad (1)$$

and allowed us to deduce the following parameters: $B_{HF}(0)$ = 487±2 kOe, T_c = 383±1 K, β = 0.23±0.01. The solid line in Fig. 5(*a*) represents the best fit of the data obtained by the least-squares procedure. These data clearly show that the magnetic phase transition occurs at 383 K. The obtained value of critical exponent β = 0.23 is lower than predicted by the classical Landau theory $\frac{1}{2}$ and is close to $\frac{1}{4}$ which **is characteristic to[?]** phase transition at the tricritical point (Huang, 1987). Another reason for such a value of the critical exponent may be the two-dimensional character of magnetic interaction. Indeed, for layered magnetic systems, close values of β are reported (Taroni *et al.*, 2008).

Two other components [green (II) and magenta (III) curves in Fig. 4] do not change significantly with an increase in temperature [Figs. 5(*b*) and 5(*c*)]. The values of the hyperfine parameters of the doublets are characteristic of the Fe^{2+} atoms. It is assumed that the doublet shown by the green curve is related to the Fe^{2+} atoms (1*f* and 2*n* crystallographic sites), while the component shown by the magenta curve is related to $Fe^{2.5+}$ (1*a* site). However, it should be noted that in order to obtain more detailed information on the cation distribution in the structure of hulsite, it is necessary to provide Mössbauer experiments at low temperatures. The values of the isomer shift and quadrupole splitting of all the components decrease with an increase in temperature [Fig. 5(*b*)]. The isomer shift values decrease due to the second-order Doppler effect, while the decrease of the quadrupole splitting is caused by a decrease of an electric field gradient due to a more uniform filling of 3d levels by resonant iron atoms at higher temperatures. However, values of the isomer shift of components I and III decrease more obviously at higher temperatures (above 600 K). An increase of values of the quadrupole splitting of component III as well as a decrease of relative area of

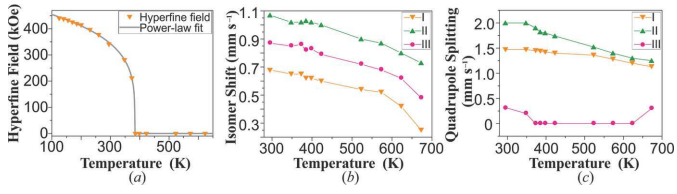

Figure 5
Temperature dependencies of the hyperfine parameters of ^{57}Fe Mössbauer spectra of hulsite: (*a*) hyperfine field of component I, (*b*) isomer shift and (*c*) quadrupole splitting.

component II is observed. In the region of higher velocities, new lines appear corresponding to the magnetic component of α-Fe_2O_3 (hematite) (Fig. 4). Such behavior of a system at high temperatures **should be caused[?]** by the Fe^{2+} oxidation. The metal cations do not change their octahedral coordination throughout the whole temperature range [Figs. 5(*b*) and 5(*c*)].

3.2. Crystal structure description

3.2.1. Crystal structure of vonsenite. In terms of cation-centered polyhedral (Fig. 6), the structure of vonsenite is described as a framework composed of vertex-sharing [O(4)] and edge-sharing [O(2)–O(2), O(2)–O(3) and O(2)–O(5)] metal–oxygen $[MO_6]^{n-}$ octahedra that form the infinite zigzag chain [Fig. 6(*a*)]. The $[BO_3]^{3-}$ isolated triangles [Fig. 6(*c*)] are connected to the octahedra by the vertices. According to the Mössbauer spectroscopy and single-crystal X-ray diffraction data (see §§2.5 and 3.1), the *M*(1) and *M*(3) positions, or the 2*a* and 4*g* crystallographic sites, are occupied by the divalent iron and magnesium atoms, the *M*(2) (2*d*) positions are occupied by $Fe^{2.5+}$, the *M*(4) (4*h*) positions are occupied by Fe^{3+} and Sn^{4+} (Tables S2). The average *M*(1)—O and *M*(3)—O bond lengths = 2.13 Å, ⟨*M*(2)—O⟩ = 2.09 Å, ⟨*M*(4)—O⟩ = 2.06 Å (Tables S4). Thus, the values of the average bond distances between the trivalent cation and oxygen are shorter than those between the divalent one and oxygen since it is known that the ionic radii r_{ion} of Fe^{2+} and Fe^{3+} in octahedral coordination are 0.78 and 0.64 Å, respectively (Shannon, 1976). The ⟨B(1)—O⟩ bond length is 1.38 Å. As the temperature increases by 100 K, an elongation of the *M*—O bonds of up to 0.02 Å is observed (Tables S4). The boron—oxygen bond lengths virtually do not change with the increase in temperature, which is in agreement with the data from the previous investigations of temperature-dependent structural changes in borates using low- and high-temperature single-crystal X-ray diffraction (Bubnova ***et al.***, 2002; Bubnova & Filatov, 2013).

In terms of the oxocentred polyhedra, the structure of vonsenite is composed of the distorted $[OM_4]^{n+}$ and $[OM_5]^{n+}$ polyhedra [Figs. 7(*a*) and 7(*b*)]. Moreover, for the first time, the $[OM_5]^{n+}$ tetragonal pyramids in the structures of vonsenite and hulsite are described (Fig. 7). In the structure of vonsenite both types of polyhedra form double chains elongated along the *c* axis [Fig. 7(*b*)]. The double chains composed of the vertex-sharing $[OM_4]^{n+}$ tetrahedra are described by Krivovichev *et al.* (1998). The second type of double chain is composed of the edge-sharing $[OM_5]^{n+}$ pyramids [Fig. 7(*b*)]. These slanted double chains are connected by common vertices and edges forming a framework.

The $[O(4)M_4]^{n+}$ tetrahedron is composed of the *M*(1), *M*(3) divalent cations and two *M*(4) cations with oxidation state of 2.5+ and 3+. The $[O(2)M_5]^{n+}$ pyramid is composed of the *M*(3) divalent cation, two *M*(2) and two *M*(4) cations with oxidation states of 2.5+ and 3+ [Fig. 7(*b*)]. The divalent *M*(3) atom is the vertex of the $[OM_5]^{n+}$ pyramid. The tetrahedra are connected to each other by the common *M*(1) and *M*(4) vertices and to the $[OM_5]^{n+}$ tetragonal pyramids by the *M*(3) vertices and *M*(4)–*M*(4) edges. The $[OM_5]^{n+}$ polyhedra are connected to each other by the common *M*(2)–*M*(2) and *M*(2)–*M*(4) edges. The O(4)—*M* bond lengths in the tetrahedra are 1.94–2.02 Å, the average O(4)—*M* bond length is 1.99 Å. The O(2)—*M* bond lengths are longer than those in the tetrahedra and equal to 2.08 and 2.09 Å, ⟨O(2)–*M*⟩ = 2.09 Å.

3.2.2. Crystal structure of hulsite. Oxidation states and cation distribution of iron and tin in hulsite were determined using Mössbauer spectroscopy (see §3.1). There are five positions of cations in the crystal structure: the *M*(1) position, or 1*a* site, is occupied by the $Fe^{2.5+}$ cations, *M*(2) (1*g*) and *M*(3) (1*d*) sites are occupied by Fe^{3+}, *M*(4) and *M*(5) (1*f* and 2*n*) by the divalent iron and magnesium atoms. These cations are surrounded by six oxygen atoms forming $[MO_6]^{n-}$ octahedra. The octahedra are connected to each other by the edges forming chains of two types. The first one is **practically**

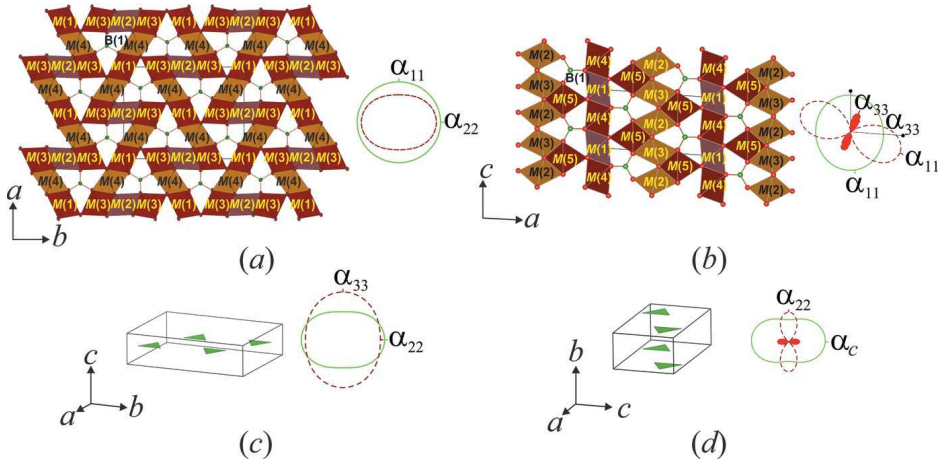

Figure 6
The wallpaper structures of (*a*) vonsenite and (*b*) hulsite represented in terms of $[MO_6]^{n-}$ cation-centered polyhedra in comparison with figures of thermal expansion. Arrangement of the $[BO_3]^{3-}$ triangles in comparison with figures of thermal expansion of (*c*) vonsenite and (*d*) hulsite (the solid green line — 300 K, the dashed red line — the maximum temperature).

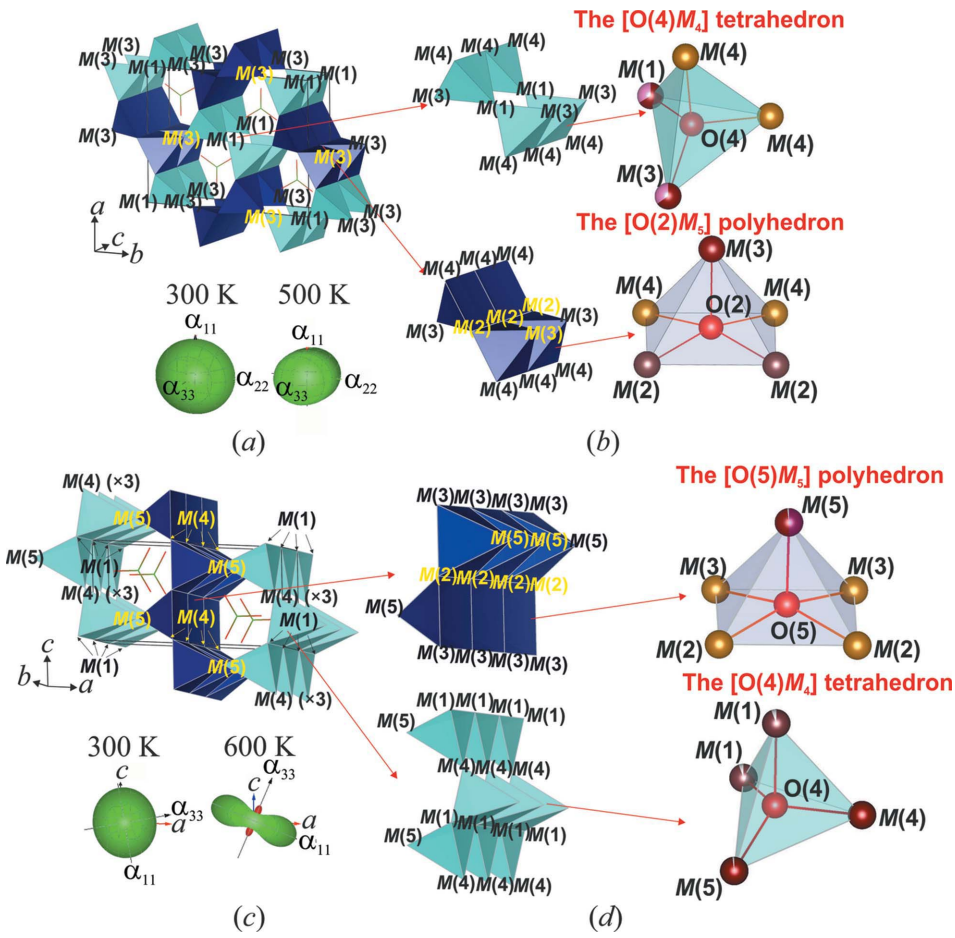

Figure 7
The crystal structures of (*a*, *b*) vonsenite and (*c*, *d*) hulsite represented in terms of the oxocentred polyhedra in comparison with figures of thermal expansion: the framework of vonsenite consists of different chains composed of the $[O(4)M_4]^{n+}$ tetrahedra and $[O(2)M_5]^{n+}$ tetragonal pyramids while the framework of hulsite consists of alternative layers composed of the $[O(4)M_4]^{n+}$ and $[O(5)M_5]^{n+}$ polyhedra. The $[OM_4]^{n+}$ tetrahedra are colored in turquoise, the $[OM_5]^{n+}$ tetragonal pyramids – in blue.

direct[?meaning] and consisted of a sequence of $[M(1)O_6]^{n-}$ and $[M(4)O_6]^{n-}$ polyhedra, and the second one is a zigzag chain consisting of $[M(2)O_6]^{n-}$, $[M(3)O_6]^{n-}$ and $[M(5)O_6]^{n-}$ octahedra [Fig. 6(*b*)]. According to single-crystal X-ray diffraction data of a hulsite reported by Yamnova *et al.* (1978), the average $M(1)-O$ bond length is 2.07 Å, $\langle M(2)-O\rangle$ and $\langle M(3)-O\rangle$ are 2.08 Å, $\langle M(4)-O\rangle$ and $\langle M(5)-O\rangle$ are 2.13 Å (Table S7). The boron atoms are surrounded by three oxygen atoms, forming the isolated triangles. The planes of the $[BO_3]^{3-}$ triangles are perpendicular to metal–oxygen layers and the triangles are connected to the octahedra by common vertices. The $\langle B(1)-O\rangle$ bond length is 1.38 Å.

Although it is possible to obtain the same chains composed of the oxocentred polyhedra, these chains form two types of layers in the *bc* plane [Figs. 7(*c*) and 7(*d*)]. The layer, which consists of the $[O(4)M_4]^{n+}$ tetrahedra, was first described by Krivovichev *et al.* (1998). The second one, which is composed of the edge-sharing pyramids, is described here for the first time. The layers are connected to each other by the common $M(5)$ vertices forming a framework. The $[O(4)M_4]^{n+}$ tetrahedra are connected to each other by the common $M(4)$ vertices and $M(1)$–$M(1)$ edges. The O(4) atoms are surrounded by two metal cations with oxidation state of 2.5+ and two divalent cations. The $O(4)-M$ bond lengths in the tetrahedra are 1.96–2.06 Å, the average $O(4)-M$ bond length is 2.02 Å. The $[O(5)M_5]^{n+}$ pyramids are connected to each other by the $M(2)$–$M(2)$, $M(3)$–$M(3)$ and $M(2)$–$M(3)$ edges. The O(5) atoms are surrounded by four metal cations with oxidation state of 3+ and one divalent cation. The $O(5)-M$ bond lengths in the $[O(5)M_5]^{n+}$ polyhedra vary from 2.07 to 2.09 Å, $\langle O(5)-M\rangle$ is 2.08 Å. The oxocentred polyhedra are interconnected by the common $M(5)$ vertices.

3.3. Thermal analysis

The DSC curve of vonsenite [Fig. S1(*a*)] shows several thermal effects. The highest peak is within the range of 1513–1590 K with a maximum at 1571 K and it corresponds to the melting of the sample. Hulsite starts to melt at approximately 1504 K [Fig. S1(*b*)]. An exothermic effect of low intensity within the range of 520–615 K in the DSC curve of vonsenite corresponds to assumed prolonged oxidation of the Fe^{2+} to Fe^{3+} oxidation in the sample, which starts at about 500 K according to the Mössbauer spectroscopy data (see §3.1.2).

The oxidation in hulsite occurs at about 600 K (see §3.1.3) and it can be seen in [Fig. S1(*b*)] (DSC curve) as an exothermic effect of low intensity within the range of 550–700 K. An insufficient mass increase by approximately three relative percent in the whole temperature range can be seen in the TG curves of the minerals (Fig. S1), which is probably caused by an increase of the oxygen content in the composition of the samples due to a prolonged solid-phase decomposition of the samples to hematite, α-Fe_2O_3, and warwickite, $(Fe,Mg)_2(BO_3)O$ (see §3.4). Fluctuations in the mass of vonsenite, which are equal to ±0.3 relative percent, cannot be interpreted correctly, because these values are in the borders of the accuracy of the determination of the weight (±2 relative percent) (see §2.4).

3.4. High-temperature X-ray diffraction

3.4.1. Thermal behavior of vonsenite. As can be seen in **Fig. S2(*a*)**, vonsenite undergoes the solid-phase decomposition caused by the oxidation started at about 500 K. At the HTXRD patterns this process is seen as appearance of peaks of α-Fe_2O_3 and **assumable[?]** X-ray amorphous B_2O_3 at 610 K (I), and then of a mixed-valent iron oxoborate warwickite, $(Fe,Mg)_2(BO_3)O$, at approximately 900 K (II) [**Fig. S2(*b*)**]. The difference between the temperatures of the oxidation determined by Mössbauer spectroscopy and HTXRD may be due to the different experimental conditions such as the heating rate. Peaks of vonsenite practically disappear after 1000 K (III). The change of the quantitative phase composition of vonsenite estimated by the Rietveld method with an increase in temperature is shown in **Fig. S3(*a*)**.

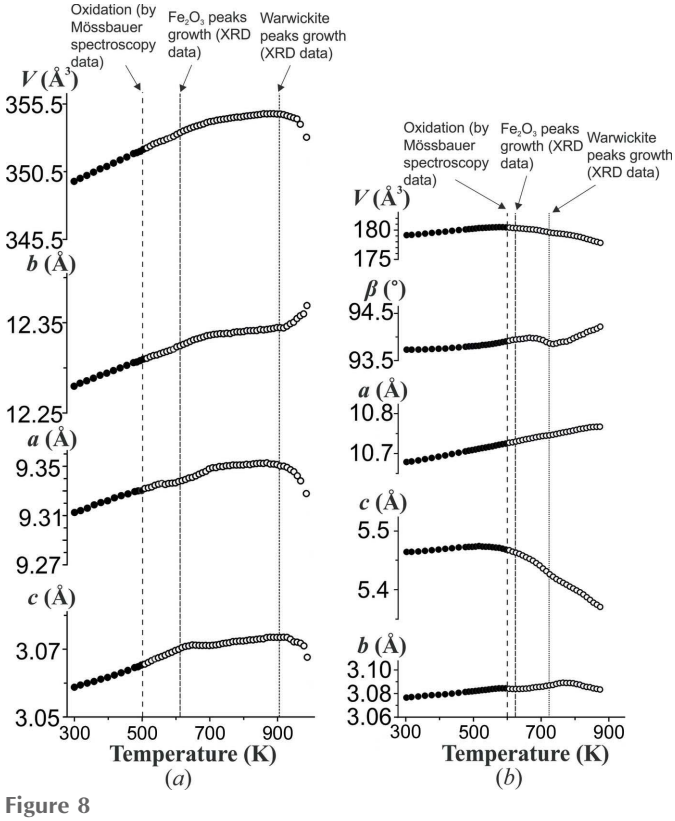

Figure 8
Temperature dependencies of the unit-cell parameters of (*a*) vonsenite and (*b*) hulsite.

Table 2
Thermal expansion coefficients of vonsenite at selected temperatures (K).

Coefficient α ($\times 10^6$ K^{-1})	300	350	375	450	500
α_a	11.91 (4)	10.74 (2)	10.66 (2)	9.59 (1)	8.27 (3)
α_b	12.81 (7)	11.87 (3)	11.78 (3)	10.93 (2)	9.86 (5)
α_c	8.32 (4)	9.86 (2)	10.01 (2)	11.39 (9)	13.14 (3)
α_V	33.1 (1)	32.5 (5)	32.6 (7)	31.9 (2)	31.3 (8)
$\alpha_{max}/\alpha_{min}$	1.5	1.2	1.15	1.2	1.6

The temperature dependencies of the orthorhombic unit-cell parameters as well as the volume [Fig. 8(*a*)] were approximated using quadratic polynomials in the temperature range 300–500 K (before the beginning of the oxidation obtained by Mössbauer spectroscopy and subsequent solid-phase decomposition) (Table S8).

The calculated thermal expansion coefficients at selected temperatures are given in Table 2.

3.4.2. Thermal behavior of hulsite. The solid-phase decomposition of hulsite begins at about 620 K (I) [**Fig. S2(*d*)**]. First, it decomposes to α-Fe_2O_3 (I), peaks of warwickite start to appear at about 730 K (II). Peaks of hulsite practically disappear after 1000 K (III). The change of the quantitative phase composition of hulsite with an increase in temperature is shown in **Fig. S3(*b*)**. It should be noted that the amount of warwickite is less (about 5 wt%) than that after the decomposition of vonsenite (about 20 wt%). As it was noted by Takéuchi *et al.* (1950), vonsenite is more structurally similar to warwickite than hulsite.

The temperature dependencies of the monoclinic unit-cell parameters as well as the volume [Fig. 8(*b*)] were approximated using quadratic polynomials in the temperature range of 300–600 K (before the beginning of the oxidation obtained by Mössbauer spectroscopy and subsequent solid-phase decomposition) (Table S8). The calculated eigenvalues of thermal expansion tensor at selected temperatures are given in Table 3.

Near the critical temperature $T_c \simeq 383$ K determined by Mössbauer spectroscopy an unusual change of thermal expansion coefficients is revealed [see α_{11} and α_{33} in Fig. S4]. This is caused by a fact that there is a minimum of values of cell parameters and β angle at approximately 330–340 K. The additional HTXRD experiment and its experimental data processing confirmed repeatability of such change of the parameters and calculated coefficients near the critical temperature.

It is **expectable to obtain[?]** an abrupt change of thermal expansion coefficients near a critical temperature, which is consistent with thermodynamics on the abrupt change of the coefficients as a second-order derivative of Gibbs energy during the magnetic phase transition (Ehrenfest, 1933). However, there is a partial magnetic ordering in hulsite that **should[?] be caused by** a quasi-two-dimensional magnetic structure. Below the critical temperature, some of planes are

Table 3
Eigenvalues of thermal expansion tensor of hulsite at selected temperatures (K).

α_{11} and α_{33} are the maximum and minimum thermal expansion coefficients in the monoclinic *ac* plane.

Coefficient α ($\times 10^6$ K^{-1})	300	305	315	325	340	350	500	600
α_{11}	14.80 (7)	14.56 (7)	14.41 (6)	14.33 (6)	14.42 (6)	14.57 (5)	17.63 (6)	19.11 (2)
$\alpha_b = \alpha_{22}$	7.45 (4)	7.52 (3)	7.61 (3)	7.75 (3)	7.91 (3)	8.06 (3)	10.51 (4)	11.56 (8)
α_{33}	12.29 (6)	13.23 (6)	13.09 (6)	12.57 (5)	11.89 (5)	11.14 (4)	−1.39 (5)	−6.93 (5)
μ_{c3} = ($\alpha_{33,c}$) (°)	82.2	72.9	62.1	45.2	36.8	32.6	23.6	23.1
α_β	0.31 (2)	0.51 (2)	0.69 (2)	1.07 (2)	1.45 (2)	1.84 (2)	7.96 (1)	10.63 (2)
α_a	13.35 (2)	13.41 (2)	13.45 (2)	13.56 (2)	13.67 (2)	13.77 (2)	15.45 (1)	16.19 (2)
α_c	14.81 (8)	14.41 (9)	14.11 (9)	13.51 (8)	12.82 (9)	12.11 (8)	1.65 (8)	−2.92 (8)
α_V	35.5 (2)	35.3 (2)	35.1 (2)	34.7 (2)	34.2 (1)	33.8 (1)	26.7 (1)	23.6 (2)

magnetically ordered, while others are not ordered. Probably, due to this reason, an abrupt change is not observed, but only the unusual one. Relation between the behavior of the crystal **lattice** and magnetic ordering **is intensively discussing[?please reword]**, and is connected with coupling between strain and order parameter (Salje, 1992; Magdysyuk *et al.*, 2014).

4. Discussion

4.1. Thermal expansion of vonsenite and hulsite

The crystal structure of vonsenite expands slightly anisotropically (Table 2). The temperature dependencies of the *a* and *b* cell parameters increase monotonously [concave dependencies in Fig. 8(*a*)] causing a decrease in the expansion along these directions. Such thermal expansion is caused by the prolonged Fe^{2+} to Fe^{3+} oxidation in the *M*(1) and / or *M*(3) positions since it is known that the ionic radius r_{ion} of Fe^{2+} is less than that of Fe^{3+} in octahedral coordination (Shannon, 1976). Thus, this process should lead to a shortening of the *M*(1)—O and / or *M*(3)—O distances. The maximum expansion is along the *c* axis, *i.e.* it is perpendicular to the planes of the $[BO_3]^{3-}$ triangles [Fig. 6(*c*)], which is consistent with the principles of the high-temperature crystal chemistry of borates (Bubnova & Filatov, 2013). Values of volume thermal expansion coefficient decrease with an increase in temperature. The decrease of the α_{11} and α_{22} coefficients, which is caused by the prolonged oxidation, as well as the expansion of the structure along the *c* axis, which is caused by the arrangement of the $[BO_3]^{3-}$ triangles, both lead to an insignificant degree of thermal expansion anisotropy $\alpha_{max}/\alpha_{min}$ (Table 2).

The structure of hulsite expands highly anisotropically (Table 3). Thermal oscillations of the $[BO_3]^{3-}$ triangles also contribute to the thermal expansion of hulsite [Fig. 6(*d*)], although, this contribution is less significant than for vonsenite. It is possible to consider the anisotropy of thermal expansion of hulsite in terms of the theory of hinge deformation of monoclinic and triclinic crystals (Filatov, 2011; Bubnova & Filatov, 2013). According to the theory, the maximum thermal expansion of monoclinic compounds should be along one of the *ac* parallelogram's diagonals if the β angle changes. In this case, while the β angle increases the maximum expansion at 600 K is along the direction that is close to the longer diagonal of the parallelogram (α_{11} = 19.11 $\times$ 10^{-6} K^{-1}) [Fig. 7(*a*)]. There is also a negative linear expansion (contraction) with an increase in temperature, which is practically along the *c* axis ($\alpha_{33} = -6.93 \times 10^{-6}$ K^{-1}) that is probably due to the Fe^{2+} and/or $Fe^{2.5+}$ to Fe^{3+} oxidation in the *M*(1), *M*(4) and/or *M*(5) positions.

Values of volume thermal expansion coefficients for both minerals that belong to a family of 3 Å wallpaper structure compounds are practically the same at 300 K and decrease with an increase in temperature due to the iron oxidation process. The anisotropy of its expansion differs significantly with an increase in temperature, in particular, due to the specific arrangement of the oxocentred polyhedra. In the structure of vonsenite, the $[OM_4]^{n+}$ and $[OM_5]^{n+}$ double chains are located practically perpendicular to each other causing the slight anisotropy of the expansion [Figs. 7(*a*) and 7(*b*)]. In the structure of hulsite, $[OM_4]^{n+}$ and $[OM_5]^{n+}$ layers alternate with each other causing the high anisotropy of the expansion in a direction that is practically perpendicular to these layers [Figs. 7(*c*) and 7(*d*)].

5. Conclusion

The mixed-valent iron oxoborates, orthorhombic vonsenite and monoclinic hulsite, belonging to a family of 3 Å wallpaper structure compounds were investigated by a set of high-temperature *in situ* methods. In terms of the oxocentred polyhedra, the structures of vonsenite and hulsite are described as the frameworks composed of $[O(4)M_4]^{n+}$ tetrahedra and $[OM_5]^{n+}$ tetragonal pyramids that form double chains and **double[?]** layers, respectively. Oxidation states and distribution of iron and tin atoms in the oxoborates were determined using Mössbauer spectroscopy and compared with EDX and X-ray diffraction data. The temperatures of the Fe^{2+} to Fe^{3+} oxidation in vonsenite and hulsite are approximately 500 and 600 K, respectively. For the first time, the partial magnetic ordering was observed in hulsite with T_C at approximately 383 K. The oxidation is accompanied by an assumed deformation of crystal structures and subsequent solid-phase decomposition to hematite and warwickite. This process is seen at the temperature dependencies of unit-cell parameters and volume as its monotonic increase (concave dependencies). Near the critical temperature, the unusual

change of thermal expansion coefficients of hulsite was revealed. Further research will be focused on understanding the reasons of such a change and it will be necessary to conduct a set of low-temperature experiments (magnetometery, heat capacity, low-temperature Mössbauer spectroscopy and X-ray diffraction). The eigenvalues of the thermal expansion tensor were calculated for the oxoborates (before the beginning of the oxidation and subsequent solid-phase decomposition). The values of volume thermal expansion coefficients of the compounds are comparable to each other. Although thermal oscillations of $[BO_3]^{3-}$ triangles contribute to the anisotropy of thermal expansion of hulsite and vonsenite, the anisotropy differs significantly with an increase in temperature and the reason for its difference is in the contribution of oxocentred $[OM_4]^{n+}$ and $[OM_5]^{n+}$ polyhedra that form different sequences of the double chains and double layers in the structures of the oxoborates. In the structure of vonsenite, the $[OM_4]^{n+}$ and $[OM_5]^{n+}$ double chains are located practically perpendicular to each other causing the slight anisotropy of the expansion. In hulsite, $[OM_4]^{n+}$ and $[OM_5]^{n+}$ layers alternate with each other causing the high anisotropy of the expansion in a direction that is practically perpendicular to these layers. The maximum expansion is along the direction that is close to the longer diagonal of the *ac* parallelogram, which is consistent with the theory of hinge deformations of the monoclinic crystals.

Acknowledgements

The X-ray diffraction experiments were performed at The Centre for X-ray Diffraction Studies (Saint Petersburg State University). The authors are grateful to Dr M. G. Krzhizhanovskaya (Institute of Earth Sciences, Department of Crystallography, Saint Petersburg State University) for conducting the high-temperature X-ray powder diffraction experiments and Dr V. L. Ugolkov (Institute of Silicate Chemistry, Russian Academy of Sciences) for conducting the thermal analysis experiments. Dr Farit G. Vagizov acknowledges the Program of Competitive Growth of Kazan Federal University funded by the Russian Government.

Funding information

The following funding is acknowledged: Russian Foundation for Basic Research (RFBR) (grant No. 18-33-00644 to Yaroslav P. Biryukov, Almaz L. Zinnatullin, Institute of Silicate Chemistry of the Russian Academy of Sciences).

References

Aleksandrov, S. M. (1998). *Geochemistry of Skarn and Ore Formation in Dolomites*. VSP BV. 288.
Aleksandrov, S. M., Malysheva, T. V. & Rodin, S. S. (1967). *Geochemistry* **10**, 1104–1110. (In Russian.)
Biryukov, Ya. P., Bubnova, R. S., Filatov, S. K. & Goncharov, A. G. (2016). *Glass Phys. Chem.* **42**, 202–206.
Biryukov, Y. P., Filatov, S. K., Vagizov, F. G., Zinnatullin, A. L. & Bubnova, R. S. (2018). *J. Struct. Chem.* **59**, 1980–1988.
Bovo, L., Twengström, M., Petrenko, O. A., Fennell, T., Gingras, M. J. P., Bramwell, S. T. & Henelius, P. (2018). *Nat. Commun.* **9**, 1999.
Bruker (2012). *APEX* and *XPREP*. Bruker AXS Inc., Madison, Wisconsin, USA.
Bubnova, R. S. & Filatov, S. K. (2013). *Z. Kristallogr. Cryst. Mater.* **228**, 395–428.
Bubnova, R. S., Firsova, V. A., Volkov, S. N. & Filatov, S. K. (2018). *Glass Phys. Chem.* **44**, 33–40.
Bubnova, R. S., Shepelev, Ju. F., Sennova, N. A. & Filatov, S. K. (2002). *Z. Kristallogr. Cryst. Mater.* **217**, 444–450.
Douvalis, A. P., Moukarika, A., Bakas, T., Kallias, G. & Papaefthymiou, V. (2002). *J. Phys. Condens. Matter*, **14**, 3303–3320.
Eakle, A. S. (1920). *Am. Mineral.* **5**, 141–143.
Ehrenfest, P. (1933). *Proc. R. Acad.* **36**, 153–157.
Filatov, S. K. (2011). *Crystallogr. Rep.* **56**, 953–961.
Filatov, S. K. & Bubnova, R. S. (2007). *Z. Kristallogr. Suppl.* 2007, 447–452. NOT CITED, REMOVE?
Filatov, S. K., Bubnova, R. S., Shepelev, Y., Anderson, J. & Smolin, Y. (2005). *Cryst. Res. Technol.* 40, 7–20. NOT CITED REMOVE?
Freitas, D. C., Continentino, M. A., Guimarães, R. B., Fernandes, J. C., Oliveira, E. P., Santelli, R. E., Ellena, J., Eslava, G. G. & Ghivelder, L. (2009). *Phys. Rev. B*, **79**, 134437.
Freitas, D. C., Guimarães, R. B., Fernandes, J. C., Continentino, M. A., Pinheiro, C. B., Resende, J. A. L. C., Eslava, G. G. & Ghivelder, L. (2010). *Phys. Rev. B*, **81**, 174403.
Gomonay, E. V. & Loktev, V. M. (2014). *Low Temp. Phys.* **40**, 17–35.
Greedan, J. E. (2001). *J. Mater. Chem.* **11**, 37–53.
Greedan, J. E. (2010). *Functional Oxides*, edited by D. W. Bruce, D. O'Hare and R. I. Walton, ch. 2, pp. 41–117. John Wiley and Sons.
Hawthorne, F. C. (2014). *Mineral. Mag.* **78**, 957–1027.
Huang, K. (1987). *Statistical Mechanics*, 2nd ed. p. 432. Wiley
Knopf, A. & Schaller, W. T. (1908). *Am. J. Sci.* **175**, 323–331.
Knyazev, Yu. V., Kazak, N. V., Nazarenko, I. I., Sofronova, S. N., Rostovtsev, N. D., Bartolome, J., Arauzo, A. S. & Ovchinnikov, G. (2019). *J. Magn. Magn. Mater.* **474**, 493–500.
Konnert, J. A., Appleman, D. A. & Clark, J. R. (1976). *Am. Mineral.* **61**, 116–122.
Krause, L., Herbst-Irmer, R., Sheldrick, G. M. & Stalke, D. (2015). *J. Appl. Cryst.* **48**, 3–10.
Krivovichev, S. V., Filatov, S. K. & Semenova, T. F. (1998). *Russ. Chem. Rev.* **67**, 137–155.
Krivovichev, S. V., Mentré, O., Siidra, O. I., Colmont, M. & Filatov, S. K. (2013). *Chem. Rev.* **113**, 6459–6535.
Larrea, J. J., Sánchez, D. R., Litterst, F. J., Baggio-Saitovitch, E. M., Fernandes, J. C., Guimarães, R. B. & Continentino, M. A. (2004). *Phys. Rev. B*, **70**, 174452.
Li, Z., Stevens, J. G., Zhang, Y. & Zeng, Y. (1994). *Hyperfine Interact.* **83**, 489–494.
Lou, Y., Li, D., Li, Z., Jin, S. & Chen, X. (2015). *Sci. Rep.* 5, 10996. NOT CITED, REMOVE?
Magdysyuk, O. V., Müller, M., Dinnebier, R. E., Lipp, C. & Schleid, T. (2014). *J. Appl. Cryst.* **47**, 701–711.
Matsnev, M. E. & Rusakov, V. S. (2012). *AIP Conf. Proc.* pp. 178–185.
Medrano, C. P. C., Freitas, D. C., Passamani, E. C., Resende, J. A. L. C., Alzamora, M., Granado, E., Galdino, C. W., Baggio-Saitovitch, E., Continentino, M. A. & Sanchez, D. R. (2018). *Phys. Rev. B*, **98**, 054435.
Medrano, C. P. C., Freitas, D. C., Sanchez, D. R., Pinheiro, C. B., Eslava, G. G., Ghivelder, L. & Continentino, M. A. (2015). *Phys. Rev. B*, **91**, 054402.
Momma, K. & Izumi, F. (2011). *J. Appl. Cryst.* **44**, 1272–1276.
Moore, P. B. & Araki, T. (1974). *Am. Mineral.* **59**, 985–1004.
Oxford Instruments (2016). *AZtec*. Oxford Instruments, Abingdon, Oxfordshire, UK
Petříček, V., Dušek, M. & Palatinus, L. (2014). *Z. Kristallogr.* **229**, 345–352.
Salje, E. (1992). *Phys. Rep.* **215**, 49–99.

Sasaki, A., Himeda, A., Konaka, H. & Muroyama, N. (2010). *Rigaku J.* **26**, 10–14.
Shannon, R. D. (1976). *Acta Cryst.* A**32**, 751–767.
Shepelev, Y. F., Bubnova, R. S., Filatov, S. K., Sennova, N. A. & Pilneva, N. A. (2005). *J. Solid State Chem.* 178, 2987–2997. NOT CITED, REMOVE?
Shimomura, S., Nakamura, S., Ikeda, N., Kaneko, E., Kato, K. & Kohn, K. (2007). *J. Magn. Magn. Mater.* **310**, 793–795.
Smith, D. L. & Zuckerman, J. J. (1967). *J. Inorg. Nucl. Chem.* **29**, 1203–1210.
Suknev, V. S. & Diman, E. N. (1975). *J. Appl. Spectrosc.* **22**, 194–196.
Swinnea, J. S. & Steinfink, H. (1983). *Am. Mineral.* **68**, 827–832.
Takéuchi, Y. (1956). *Mineral. J.* **2**, 19–26.
Takéuchi, Y., Watanabé, T. & Ito, T. (1950). *Acta Cryst.* **3**, 98–107.
Taroni, A., Bramwell, S. T. & Holdsworth, P. C. W. (2008). *J. Phys. Condens. Matter*, **20**, 275233.
Vallejo, E. & Avignon, M. (2007). *J. Magn. Magn. Mater.* **310**, 1130–1132.
Whangbo, M., Koo, H. J., Dumas, J. & Continentino, M. A. (2002). *Inorg. Chem.* **41**, 2193–2201.
Yamnova, N. A., Simonov, V. A. & Belov, N. V. (1978). *Dokl. Akad. Nauk SSSR*, **238**, 1094–1097.